J Musculoskelet Neuronal Interact 2005; 5(4):369-378

Hylonome

Poster abstracts from the 35th Meeting of the International Sun Valley Workshop on Skeletal Tissue Biology

July 31-August 3, 2005, Sun Valley, Idaho, USA

Program Chairman: David B. Burr

Abstract No.	Topic
P1-19	Poster abstracts (Authors marked with an asterisk (*) are Recipients of the Alice L. Jee Travel Award)

P-1

Both Risedronate and PTH Maintain Bone Mechanical Properties and Matrix Composition in a Mouse Model of Glucocorticoid-Induced Osteoporosis

*G. Balooch[1], W. Yao[2], R.K. Nalla[3], R.O. Ritchie[3], J.H. Kinney[1], M. Balooch[1], N.E. Lane[2]
[1]University of California, San Francisco, CA, USA; [2]University of California, Davis, CA, USA; [3]LawrenceBerkeley National Laboratory, Berkeley, CA, USA
E-mail: gbalooch@yahoo.com

Glucocorticoid-induced osteoporosis (GIOP) commonly results from suppression of bone formation and enhancement of bone resorption, which alters bone structure and induces bone fragility. Bisphosphonates, acting as anti-resorptive agents, and anabolic agents, are effective therapies in the prevention and treatment of GIOP in clinical trials; however, the mechanism by which they increase bone strength is not yet clear. The purpose of this study was to assess if concurrent treatment of mice with GCs+Risedronate (RIS) or GCs+PTH would maintain bone mechanical properties (local and global) and bone mineral concentration (BMC) compared to GC treatment alone. Four groups of mice were randomized to placebo, GC (1.5mg/kg in a slow release pellet that was s.c. implanted x 21 days), GC+RIS (5μg/kg, sc, 5X/wk) and GC+hPTH (1-34) (40μg/kg, sc, 5X/wk- and treated for 21 days). After sacrifice, the following procedures were done: microCT for trabecular microarchitecture and compression tests of 3rd LVB. The 4th LVB were processed for Elastic Modulus Mapping (EMM), a scanning probe microscopy-based technique that allows high resolution (15nm) mapping of elastic modulus (E) surrounding osteocyte lacunae. In addition, synchrotron X-ray tomography (XTM) analysis was performed on femurs to assess changes in BMC. Finally, EMM and XTM were performed on iliac crest biopsies from GC and GC+RIS-treated subjects. Treatment with GCs reduced BV/TV by 53% and both GC+RIS and GC+PTH treatment prevented loss of BV/TV. Compared to the PL group, E was reduced by 66% and 58% in GC-treated mice ($p<0.001$) and humans ($p<0.05$), respectively, along the trabeculae perimeter and surrounding the osteocyte lacunae; however, E was maintained with GC+RIS and GC+PTH groups. Compression tests of the LVB3 in mice treated with GC+PTH and GC+RIS revealed a 62% and 88% increase in strength ($p<0.001$), 64% and 61% increase in compression modulus ($p<0.001$), and 51% and 39% increase in stiffness ($p<0.01$), respectively, compared to PL mice. XTM analysis revealed a 45% and 31% reduction in BMC in the trabeculae of both GC-treated mouse ($p<0.01$) and human bone ($p<0.01$), respectively, while GC+RIS and GC+PTH treatment led to a 33% ($p<0.01$) and 48% ($p<0.01$) increase in BMC compared to PL, respectively. These results indicate that PTH and RIS treatments in the presence of GCs prevent the deterioration of BMC and both local and global mechanical properties. Therefore, these therapies, albeit through different mechanisms, appear to be effective means in reducing bone fragility in GC-treated individuals.

The authors have no conflict of interest.

P-2

Biomechanical Analysis of pQCT Indicators of Bone Mass, Mineral Density, Design and Strength in Forearms and Legs of Normal Men and Pre- and Post-MP Women

R. Capozza, G. Cointry, S.E. Ferretti, S. Feldman, N.M. Fracalossi, L. Sarrió, P. Reina, M.V. Ferretti, M. Ferullo, G. Marchetti, J.L. Ferretti
Center for P-Ca Metabolism Studies (CEMFoC), Fac of Medicine, Natl Univ of Rosario, Argentina
E-mail: jlferretti@arnet.com.ar

The aim of this study was to describe the interrelationships between different bone properties and the interaction of regional muscles with their biological determination, employing pQCT.

With this purpose, the natural associations between indicators of bone mass (BMC, cortical area, trabecular density), design (CSMIs), mineral density (cortical vBMD) and strength (BSIs) and of muscle strength (CSA) determined by pQCT in forearms (4 and 66% sites) and legs (4, 14, 38 and 66% sites) of 40 men, 60 pre-MP women and 100 post-MP women aged 25-85a, were analyzed following biomechanical criteria.

Indicators of bone mass, design and strength were higher in men than in pre-MP women. Mass and strength (not design) indicators decayed significantly after MP. Cortical vBMD, higher in women than men, decayed more dramatically than the other indicators after MP. *Distribution/mass* (MI/CortCSA) and *distribution/quality* (MI/CortvBMD) curves showed that MIs tended to stabilize after MP, despite the bone mass reduction. The intracortical distribution of vBMD felt dramatically after MP, showing also a geometrical discontinuity of the areas of highest-density voxels (>1.0 cm^{-1} attenuation threshold). In agreement with predictions according to known inter-regional biomechanical relationships, the total BMC assessed at the 4% site in the legs was the same as that determined at the 38% site and 1.5 times that determined at the 14% site in all groups. Indicators of bone mass, design and strength correlated with muscle area in both 66% sites showing common, saturation relationships for men and pre-MP women, and a lower slope for post-MP women.

These results suggest that (1) Bone mass varies allometrically with body size and biomechanically with the regional muscle strength in fertile individuals, indicating that the method could evaluate the biomechanical control of bone modeling by bone mechanostat. (2) Estrogen deficiency determines a loss of

mass and especially mineralization of cortical bone (enhanced microporosity induced by stimulation of Haversian remodeling), maintaining the diaphyseal design relatively stable, thus slowing (yet not completely preventing) the development of bone fragility. (3) Bone *mechanostat* remains healthy (yet metabolically disturbed) after MP; hence, the status of this system should be also evaluated for diagnosing osteoporosis, avoiding to establish this diagnosis based only on the severity of the osteopenic condition (DXA-BMD t-scores). (4) Comparison of BMC between predominantly trabecular or cortical sites in the same individual would allow detecting a relative deterioration of the former compared to the latter, as determined in "systemic" (primary or endocrine-metabolic) osteopenias. (5) In practice, a *Z-scorization* of the described natural relationships will provide suitable reference charts for an original, biomechanical diagnosis of osteoporosis, and a differential diagnosis between "disuse" and "systemic" osteopenias (disuse would correspond to a normal bone/muscle proportionality, while a systemic disturbance would tend to reduce both the bone/muscle proportionality and the trabecular/cortical bone mass ratio), with important therapeutic implications (exercise in the first case, drugs or hormones in the second one).

The authors have no conflict of interest.

P-3

Determination of Carrier Status in ADO2: An *In Vitro* Study of Clinically Unaffected Gene Carriers

*K. Chu, R. Snyder, M.J. Econs
Department of Medicine, Indiana University School of Medicine, Indianapolis, IN, USA
E-mail: kachu@iupui.edu

Autosomal dominant osteopetrosis type II (ADO2) is a heritable osteosclerotic disorder that results from heterozygous mutations in the ClCN7 gene. However, of those individuals with a ClCN7 mutation, 1/3 are asymptomatic carriers. Disease severity in the remaining 2/3 is highly variable. The most severely affected manifest multiple fractures, osteomyelitis, visual loss and, occasionally, bone marrow failure. There is no genotype/ phenotype correlation and families frequently have both carriers and severely affected individuals.

To determine whether the carrier status results from the bone microenvironment (i.e., secretion of cytokines, hormonal environment, and condition of the other bone cells) or is intrinsic to the osteoclasts, we performed *in vitro* osteoclast cell culture in affected patients, carriers and normal controls (n=5 in each group). Subjects were matched for age, sex and ethnicity. Human peripheral blood mononuclear cells were isolated by magnetic beads and differentiated into osteoclasts by stimulation with hRANK-L and hM-CSF. Cell fusion, F-actin ring formation, TRAP activity, cell acidic microenvironment analysis were investigated and no significant difference was found between the three groups. However, osteoclasts from the carrier and normal groups generated more extensive and continuous resorption pits compared to the affected groups, which had rare and restricted pits. Moreover, the pits from the carrier and the normal groups formed much earlier and extended much more rapidly than the pits from the affected groups. There were no significant differences between the carrier and normal groups at any time point.

In conclusion, osteoclasts from the carriers, in contrast to those from the affected individuals (who had the same ClCN7 mutations) function normally in cell culture. This finding supports the hypothesis that intrinsic osteoclast factors determine whether an individual with a ClCN7 mutation becomes an affected patient or an asymptomatic carrier. Further understanding of this mechanism is likely to lead to the development of new approaches for the treatment of affected patients.

The authors have no conflict of interest.

P-4

Comparison of Osteon Histomorphometry in Human Ribs to Equine Appendicular Bones

G.C. Clark, S.M. Sorenson, K. Taylor, J. Hoopes, J.G. Skedros
University of Utah Department of Orthopaedic Surgery, SLC, UT, USA
E-mail: jskedros@utahboneandjoint.com

Introduction. Data regarding osteonal remodeling in human ribs have been broadly extrapolated to appendicular bones of various mammalian species. However, ribs have notable differences when compared to appendicular long bones; ribs 1) are derived from sclerotomes of the somites, in contrast to limb bones that are derived from lateral plate mesoderm, 2) are phylogenetically primitive, occurring in the fossil record much earlier than limb bones, 3) are metabolically more active and sensitive to hormonal changes such as during lactation, and 4) receive frequent and low-strain loading; e.g., loading occurs even when the animal is recumbent. The present study is the second (the first study examined horse radii) of a series of investigations assessing the appropriateness of using osteonal rib data for broad extrapolations to limb bones. In view of these differences, the

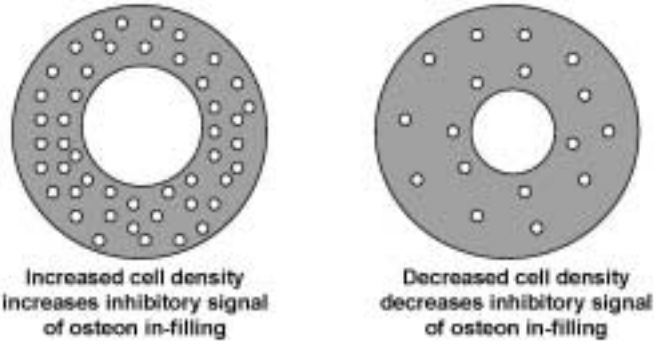

Figure 1. Two osteons showing the relationships of cell density with osteonal in-filling/bone formation.

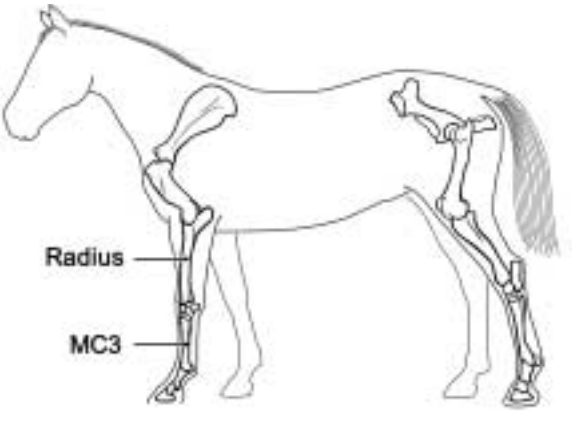

Figure 2. Horse skeleton showing bone types used.

		Human Rib			Equine Radius			Equine MC3		
		On.Ar	Lc.N/ On	Lc.N/ B.Ar	On.Ar	Lc.N/ On	Lc.N/ B.Ar	On.Ar	Lc.N/ On	Lc.N/ B.Ar
Hc.Ar	r	0.64	0.56	~	0.47	0.34	~	0.79	0.01	~
	p	<0.01	<0.01	~	<0.01	<0.01	~	<0.01	0.55	~
Hc.Pm	r	0.67	0.58	~	0.49	0.36	~	0.72	0.10	~
	p	<0.01	<0.01	~	<0.01	<0.01	~	<0.01	<0.01	~
Hc.Pm/ B.Ar	r	0.70	~	0.14	-0.60	~	0.43	-0.10	~	0.48
	p	<0.01	~	<0.01	<0.01	~	<0.01	<0.01	~	<0.01
Lc.N/ On	r	0.93	~	~	0.79	~	~	0.48	~	~
	p	<0.01	~	~	<0.01	~	~	<0.01	~	~
Lc.N/ B.Ar	r	0.14	~	~	-0.32	~	~	-0.23	~	~
	p	<0.05	~	~	<0.01	~	~	<0.01	~	~
Hc.Ar/ On.Ar	r	~	~	0.10	~	~	0.31	~	~	0.37
	p	~	~	<0.05	~	~	<0.01	~	~	<0.01

Results Table

present study further tests the hypothesis presented in Figure 1, which shows two osteons. The hypothesis that increased osteocyte densities correlate with reduced osteon in-filling reflects the idea that these cells form a network that represses osteonal bone formation (Martin, 2000).

Methods. 50X backscattered electron images were obtained from mid-third diaphyses of 10 mature (ages 2-10) equine third metacarpals (MC3s) and radii from mixed breeds (**MC3s:** in eight radial sectors: dorsal, dorsal-lateral, lateral, palmar-lateral, palmar, palmar-medial, medial, and dorsal-medial; **Radii:** cranial, caudal, medial, and lateral cortices). Using the histomorphometry parameters examined by Qiu et al. (2003) in human male ribs, approximately 2,470 (MC3s) and 2,350 (horse radii) osteons were examined for osteonal area (On.Ar), osteonal bone area (B.Ar), central (Haversian) canal area (Hc.Ar) and perimeter (Hc.Pm), number of osteocyte lacunae per osteon (Lc.N/On) and osteonal bone area (Lc.N/B.Ar), and the Haversian canal perimeter to osteonal bone area ratio (Hc.Pm/B.Ar). According to the ASBMR Histomorphometry Nomenclature Committee (Parfitt et al., 1987), the 2-D parameters (B.Ar and Hc.Pm) in osteons can be defined as the 3-D parameters as the BS/BV ratio. Thus Hc.Pm/B.Ar can be regarded as the bone surface to bone volume (BS/BV) ratio (Qiu et al., 2003). The data in this study are compared to human rib data (mature males) reported by Qiu et al. (2003).

Results (see table). Equine MC3 data: Results showed that, similar to human ribs, On.Ar in the equine MC3s had a strong positive correlation with Hc.Ar and Hc.Pm ($r = 0.79, 0.72$; $p < 0.01$, respectively). However, in contrast to human ribs, Lc.N/On showed little, if any, correlation to Hc.Ar and Hc.Pm ($r = 0.01, 0.10$; $p < 0.01$, respectively) in the MC3s.

Equine Radius data: Equine radii showed lower correlation (but still positive and statistically significant) of On.Ar to Hc.Ar and Hc.Pm ($r = 0.47, 0.49$; $p < 0.01$, respectively) than human ribs. Furthermore, compared to human ribs, horse radii showed lower correlation of Lc.N/On to Hc.Ar and Hc.Pm ($r = 0.34, 0.36$; $p < 0.01$, respectively).

Analysis of all data in each bone revealed that BS/BV (Hc.Pm/B.Ar) was highest in the MC3, next highest in horse radii, and lowest in human ribs ($p < 0.001$ for each paired comparison). Additionally, Lc.N/On was significantly lower in the MC3 than in the horse radius and human rib ($p < 0.001$).

Discussion. These results suggest that the putative coordination between the formation of an "optimal" Haversian canal and osteocytes found in human ribs (Qiu et al., 2003) is present but weak in horse radii and virtually non-existent in the MC3s as indicated by the low correlation co-efficients comparing Lc.N/On to Hc.Ar and Hc.Pm. These relationships may not exist in bones where there are large regional variations in strain gradients and/or a highly non-uniform strain distribution, which produce relatively greater regional variations in trans-cortical fluid flow. For example, the MC3 exhibits dramatic trans-cortical strain gradients; the cranio-lateral cortex experiences ~50x less strain than the caudal-medial cortex (Gross et al., 1992). Regions of bones experiencing high strain gradients may also have more efficient nutrient delivery, which may explain why the MC3s have greater Hc.Pm/B.Ar but lower Lc.N/On than horse radii and human ribs. Beyond interspecies differences, there may be other important considerations when attempting to extrapolate human rib data to other mammalian appendicular bones. For example, it is possible that thresholds for metabolic activity of bone cells in ribs may be fundamentally different when compared to cells in appendicular bones. Rib bone is exquisitely sensitive to hormonal changes associated with lactation and appendicular bones are not. Although this is gender specific (i.e., occurs in females) it illustrates how metabolic demands can affect osteonal histomorphology in some regions differently from others. Reasons for these differences are not fully understood but do point out that histomorphometric data considered "optimal" in human ribs might not apply to other mammalian appendicular bones.

References

1. Gross TS, McLeod KJ, Rubin CT. Characterizing bone strain distribution *in vivo* using three triple rosette strain gauges. J Biomech 1992; 25:1081-1087.
2. Martin, RB. Toward a unifying theory of bone remodeling. Bone 2000; 26:1-6.
3. Qiu S, Fyhrie DP, Palnitkar S, Rao DS. Histomorphometric assessment of Haversian canal and osteocyte lacunae in different-sized osteons in human rib. Anat Rec 2003; 272A:520-525.

The authors have no conflict of interest.

P-5

Structural Properties of Florida Manatee Ribs

K.B. Clifton[1], J.J. Mecholsky Jr[2], R.L. Reep[1]
Departments of [1]Physiological Sciences and [2]Materials Science and Engineering, University of Florida, Gainesville, FL, USA
E-mail: cliftonk@mail.vetmed.ufl.edu

On average, 25% of all Florida manatees that die each year are killed by boats. Boat strikes account for 85% of deaths attributed to humans. Reducing watercraft-related mortality is a high priority in state and federal manatee recovery efforts, which focus primarily on regulating boating activities. In order to establish safe boat speeds for manatee protection, an estimate of the forces required to fracture their bone is needed. The goal of this project is to estimate the mechanical properties of whole manatee ribs. Impact tests were used to estimate the load required to initiate a fracture, and the amount of energy needed to fracture whole ribs. Manatee ribs from the mid-thoracic region were impacted with an air cannon. Fractographic analysis was applied to the fracture surfaces to calculate the loads that led to failure. Loads ranged from 91-173 MPa. Strain gauges were used on some ribs to validate these calculations. Fractal geometry was used to calculate the fractal dimensional increment (D*), a quantitative measure of the topography of an irregular fracture surface. D* is directly related to the fracture energy of a material; the higher D*, the greater the fracture energy. Results indicated D* for manatee bone (.08-.22) is at the lower end of the range for ceramics, suggesting a low amount of energy is needed to cause fracture. These impact tests will allow us to determine whether the kinetic energy generated by typical watercraft under normal operation is sufficient to fracture manatee ribs.

The authors have no conflict of interest.

P-6

Re-establishment of Normal Cancellous Bone Turnover Differs Following The Withdrawal of Alendronate and Risedronate Treatment in Ovariectomized Rats

*R.K. Fuchs, D.B. Burr
Indiana University Medical School, Indianapolis, IN, USA
E-mail: rfuchs@iupui.edu

It has been suggested that alendronate (ALN) and risedronate (RIS) have different skeletal pharmacokinetics, with ALN having a longer terminal half-life than RIS. The aim of this study was to investigate the skeletal response to the withdrawal of RIS and ALN using an ovariectomized (ovx) animal model. We hypothesized that normal bone turnover rates would be re-established sooner following the withdrawal of bisphosphonate therapy in ovx rats treated with RIS than in those treated dose-equivalently with ALN. Female Sprague Dawley rats (n=210) were ovariectomized and treated 3x/wk for 8 wks with either saline-vehicle (CON), ALN (2.4 μg/kg), low-dose RIS (1.2 μg/kg: RISlow), or high-dose RIS (2.4 μg/kg: RIShigh) via subcutaneous injection. Doses of ALN and RIS were based on clinical dose levels (on an oral mg/kg basis) and on doses known to inhibit bone loss in ovx rats. From a clinical perspective, 1 remodeling cycle is equal to ~1 month in rats and ~4-6 months in humans. Fluorochrome label (calcein) was administered 10 and 4 days prior to sacrifice for histological measurements. Animals (10/group) were sacrificed at 0, 4, 8, 12 and 16 wks after treatment withdrawal. Indices of bone turnover were significantly suppressed in all drug-treated groups compared to vehicle-treated CON after 8 wks of treatment (all $P<0.05$), and BMD of the distal femur increased significantly in all drug-treated groups after 8 wks of treatment compared to vehicle-treated CON ($P<0.05$). Trabecular bone turnover in the RISlow and RIShigh groups increased steadily following the withdrawal of treatment. In contrast, trabecular bone turnover in the ALN-treated groups did not demonstrate increases in bone turnover at any time point during treatment withdrawal. The ALN-treated groups remained significantly lower than vehicle-treated CON at all time points ($P<0.05$). At 16 wks the RIS treated groups were not significantly different from vehicle-treated CON ($P>0.05$) and there were no significant differences between the

drug-treated groups. ($P>0.05$). Normal trabecular bone turnover is re-established sooner in animals treated with RIS compared to ALN. Specifically, bone formation rates remained significantly lower in trabecular bone of the proximal tibia in ALN-treated animals than non-treated controls through 16 wks after stopping treatment, while those treated with either dose of RIS demonstrated a gradual recovery of normal bone formation rates. Outcomes from this study may have important implications for designing effective therapies for the treatment and prevention of osteoporosis.

The authors have no conflict of interest.

P-7

Role of FGF-2 in Muscle-Bone Interactions

M. Hamrick, C. Pennington, H. Chen, C. Isales, P. McNeil
Medical College of Georgia, Augusta, GA, USA
E-mail: mhamrick@mail.mcg.edu

It is now well documented that FGF-2 is anabolic to bone. Systemic injections of recombinant FGF-2 into rats increases endosteal bone formation[1], and mice with a disruption in the FGF-2 gene show decreased bone mass and bone formation[2]. FGF-2 regulates bone formation by binding to FGF receptors (FGFRs) expressed in osteoblasts and activating MAP kinase signal transduction[3]. The MAPK pathway is now known to be important for activation and phosphorylation of Cbfa1/Runx2, a transcription factor that plays a critical role in osteoblast differentiation.

If FGF-2 is responsible for adult bone anabolic responses *in vivo*, then what is the source of its production? Our work has shown that mechanical stresses generated within active skeletal muscle by exercise cause the disruption of individual myocyte plasma membranes, leading to the release of FGF-2 from these 'wounded' myocytes. Considerable data from studies of cardiac and skeletal muscle suggest a causal coupling of cell membrane disruption and hypertrophy of the associated tissue. The key concept is that a plasma membrane disruption constitutes a mechano-transduction event[4]. Signals such as growth factors are released through a disruption into extracellular spaces, where they can then stimulate cell division and/or hypertrophy in the releasing as well as neighboring cells. Fibroblast growth factor (FGF) 1 and 2 lack a signal sequence for export via the classical exocytotic pathway, yet clearly are growth stimulatory when added to the medium (or extracellular space) of responsive cell types[5]. If FGF-1 and 2 act as growth factors *in vivo*, how are they released from cells as is required for effecting this growth-promoting role? We propose that FGF-2 released from skeletal muscle acts as a local anabolic bone stimulus, coupling these two tissues in an anabolic response to a mechanical stimulus, such as exercise.

We used mice lacking FGF-2 to test the hypothesis that the osteogenic effects of muscle activity and exercise on bone are mediated by FGF-2 signaling. Normal mice and FGF-2 deficient mice (Jackson Lab, Bar Harbor, ME) were exercised on a Columbus Instruments Exer-3/6 treadmill at a rate of 12 m/min for 30 minutes a day, 5 days a week, for 4 weeks beginning at two months of age. A second group of normal mice and FGF-2 deficient mice were not exercised and were used as sedentary controls. DEXA densitometry (PIXImus system) was used to measure whole-bone mineral content (BMC) and mineral density (BMD) from the left femur. Right femora of mice were thawed in cold water at room temperature for 1 hour and then prepared for mechanical testing in 3-point anteroposterior bending using a Vitrodyne V1000 Materials Testing system. Femora were mounted on stainless steel fixtures spaced 5 mm apart, 2.5 mm either side of center. Testing was linear displacement control with a displacement rate of 0.10 mm/sec using a Transducer Techniques 5 kg load cell. Femora were loaded to failure with data points recorded every 0.01 sec. Structural, or extrinsic properties, such as ultimate force (Fu; height of curve), stiffness (S; slope of curve), ultimate displacement (du; width of curve), and energy to fracture (U; area under curve) were calculated from load-displacement curves[6].

Whole-femur bone mineral content and density increased significantly in exercised wild-type mice, but exercise had no effect on bone mass in the FGF-2 deficient mice (Figure 1). Biomechanical testing data also show that exercise had no effects on the extrinsic biomechanical properties of the bones in FGF-2 knockout mice (Table 1). These findings suggest that absence of FGF-2 signaling attenuates the osteogenic response observed with exercise, and that FGF-2 may play a significant role in bone mechanotransduction and muscle-bone interactions.

Parameter	Sedentary (n=5)	Exercised (n=5)	P-value (ANOVA)
Ultimate force (Fu; N)	32.4 (2.0)	30.2 (2.1)	ns
Displacement (du; mm)	0.36 (0.05)	0.32 (0.02)	ns
Stiffness (S; N/mm)	90.9 (12.0)	94.1 (22.2)	ns
Energy-to-fracture (U; N-mm)	5.9 (1.2)	4.8 (1.1)	ns

Table 1. Biomechanical testing results from femora of sedentary and exercised FGF-2 deficient mice. Means are shown with standard deviations in parentheses.

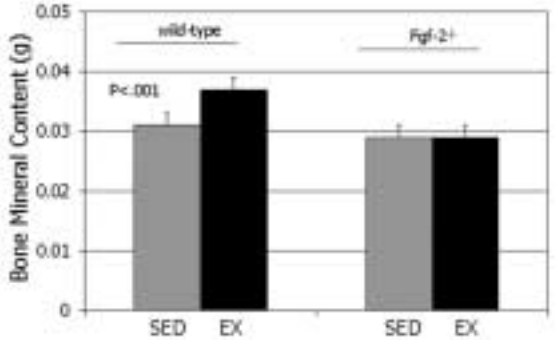

Figure 1. Graph of bone mineral content values from femora of sedentary (sed) and exercised (ex) wild-type and FGF-2-deficient mice. Note that loss of FGF2 function ablates the increase in bone mass normally observed with exercise.

References

1. Pun S, Florio CL, Wronski T. Anabolic effects of basic fibroblast growth factor in the tibial diaphysis of ovariectomized rats. Bone 2000; 27:197-202.
2. Montero A, Akada Y, Tomita M, Ito M, Tsurukami H, Nakamura Y, Doetschman T, Coffin J, Hurley M. Disruption of the fibroblast growth factor-2 gene results in decreased bone mass and bone formation. J Clin Inv 2000; 105:1085-1093.
3. Hurley M, Marcello K, Abreu C, Kessler M. Signal transduction by basic fibroblast growth factor in rat osteoblastic Py1a cells. J Bone Miner Res 1996; 11:1256-1263.
4. Grembowicz KP, Sprague D, McNeil PL. Temporary disruption of the plasma membrane is required for c-fos expression in response to mechanical stress. Mol Biol Cell 1999; 10:1247-1257.
5. Gospodarowicz D. Fibroblast growth factor. Crit Rev Oncog 1989; 1:1-26.
6. Turner CH. Biomechanics of bone: determinants of skeletal fragility and bone quality. Osteoporos Int 2002; 13:97-104.

The authors have no conflict of interest.

P-8

Elastic Modulus and Mineral Content of Fin Whale Bullae Measured by Nanoindentation and Backscattered Imaging

*S.S. Huja and S.L. Woodard
Section of Oral Biology and Orthodontics, College of Dentistry and Division of Biostatistics, College of Medicine, The Ohio State University, Columbus, OH, USA
E-mail: huja.1@osu.edu

Introduction. A wide range of elastic moduli (5-35 GPa) for mineralized tissue have been reported in the literature. The whale bulla is a highly mineralized and is not load-bearing structure. The purpose of this study was to a) estimate the indentation modulus and mineral content of fin whale bulla

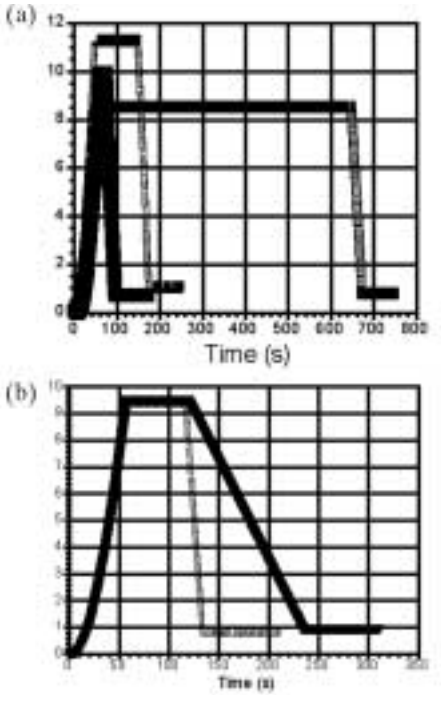

Figure 1. Schematic of Load vs. Time curves depicting (a) 10 s, 100 s and 600 s hold times and (b) 25% vs. 150% unloading rate.

	Hold Period (s)	n, indents	Mean Indentation Modulus ± SD GPa
Specimen 1	10	43	44.9 ± 5.5
	100	49	43.9 ± 4.5
Specimen 2	10	43	41.6 ± 3.7
	100	50	39.0 ± 4.6
	360	15	42.9 ± 6.0
	480	15	41.7 ± 4.1
	600	25	40.3 ± 5.9

Table 1

Unloading Rate	n, indents	Mean Indentation Modulus ± SD GPa
25%	25	39.6 ± 5.3
50%	25	37.2 ± 2.5
150%	25	38.1 ± 5.1

Table 2

	Mean WMGL ± SD
Specimen 1	180.8 ± 1.6
Specimen 2	171.8 ± 2.3

Table 3

(*balaenoptera physalus*) by nanoindentation and backscattered imaging b) examine the effects of variation in loading protocol during nanoindentation on the estimated indentation modulus of the fin whale bulla.

Methods. The whale bulla specimen was received in the dry state. Sectioning of the brittle bulla resulted in two fragments, one being slightly larger than the other. Each specimen was secured with super glue onto a custom-made polycarbonate specimen holder. The specimen was polished and sonicated. The polycarbonate specimen holder containing the polished bone specimen was inserted into the receiving table of the indentation system (Nano-XP, MTS, Oakridge, TN). Prior to a set of indents on each specimen, indents were made on a fused silica standard to ascertain calibration of the machine and diamond tip. Indents were made on the bone specimen at a rate of 10 nm/s and to a target depth of 500 nm with a Berkovich diamond indenter using established protocols. However, in this study, the hold period at peak load and the unloading rate were varied. Typically, a 5X5 array of indents was made at a particular location, with 30 mm between each indent. Specimen 1 was the smaller specimen and a 10 s or 100 s hold period was imposed at peak load. On specimen 2, repeated indents were made and a hold period at peak load of 10 s, 100s, 360 s, 480 s, and 600 s was imposed (Figure 1a). On Specimen 2, we also varied the unloading rate to be 25%, 50% or 150% of the loading cycle and during this test a 1 min. hold period at peak load was imposed (Figure 1b). After indentation, the bulla specimen was removed from the polycarbonate holder and prepared for backscattered imaging. The specimen was carbon coated and imaged on a scanning electron microscope (SEM) (XL-30 ESEM FEG, Philips, Eindhoven, Netherlands) equipped with a backscattered detector. From each of two digital images/specimen, multiple weighted mean gray level (WMGL) measurements were made (Scion Image v. 4.02, Maryland) to represent the area of interest. The data were analyzed using ANOVA with Bonferroni correction for pair-wise comparison.

Results. Specimen 1 and 2 had significantly different indentation moduli ($p<0.001$). Within specimen 1, there was no difference between the 10 s vs. the 100 s hold period. Within specimen 2, only the 10 s and 100 s modulus were different ($p=0.012$). However, all other hold periods were not significantly different from each other (Table 1).

For the unloading rate, only the modulus from the 25% and 50% unloading rate were different ($p=0.03$) from each other (Table 2). The WMGL (Table 3) for Specimen 1 and 2 were significantly different ($p<0.001$). During this scanning session, images of deer antler were obtained and the WMGL were approximately 90.

Discussion. A limitation of this study is the sample size, thus the results are only valid for the specimens tested. Whale bulla is difficult to obtain however, the mineral content and mechanical of whale bulla is of great interest. Nanoindentation tests of whale bulla have not been conducted. This is important as nanoindentation measures indentation properties over small volumes and a better relationship between mineral content and mechanical properties is more likely at this resolution. Understanding the mechanical property and mineral content interaction is important in understanding crack propagation and fracture in bone.

A range of mean indentation modulus (37-45 GPa) was estimated from the two dry whale bullae specimens. These values are slightly higher to moduli values obtained by conventional mechanical tests for determining elastic modulus[1]. We are uncertain as to the differences in the indentation moduli between the two specimens from the same whale bulla. However, the orientation of the tested surface was unknown and may have played a role in the estimated indentation modulus. Differences in hold time at peak loads do not seem to play a major role in estimating moduli of this highly mineralized tissue. However, these differences may be more important for tissues of low mineral content. Differences were seen in moduli values between the 25% and 50% unloading rates but not between the 25% and 150% and 50% and 150%. As these indents are made on different areas, it is possible that the indentation modulus of the small regions are different, because the bone tissue is not homogenous. The WMGL of the whale bulla as determined by backscattered imaging was similar to those reported in other studies[2]. Using a combined approach of WMGL and estimated indentation

modulus may allow a better understanding of structure function relationship in mineralized tissues.

Acknowledgements

Supported by College of Dentistry start up funds. Dr. R.D. Bolebaum generously provided the whale bulla specimen.

References

1. Currey JD. The effect of porosity and mineral content on the Young's modulus of elasticity of compact bone. J Biomech 1988; 21:131-139.
2. Vajda EG, Skedros JG, Bloebaum RD. Consistency in calibrated backscattered electron images of calcified tissues and minerals analyzed in multiple imaging sessions. Scanning Microscopy 1995; 9:741-755.

The authors have no conflict of interest.

P-9

Low Mineral Content Bone Has Large Differences in Elastic Properties When Tested Under Dry and Moist Conditions by Nanoindentation

*S.S. Huja and F.M. Beck
Section of Oral Biology and Orthodontics, College of Dentistry, The Ohio State University, Columbus, OH, USA
E-mail: huja.1@osu.edu

Introduction. Elastic properties of bone tissue from the appendicular skeleton have been measured under dry and moist conditions. Indentation tests indicate that measurement under moist conditions results in lowering of the indentation elastic properties by approximately 10-15%[1,2]. While these results are valid for bone of normal mineral content, similar measurement of indentation properties in low mineral content bone by nanoindentation has not been reported. It is important to investigate the relationship between dry and moist testing environments in lower mineral content bone. Deer antler mineral content has been estimated by measuring ash content and quantitative backscattered imaging. The elastic properties of deer antler have been measured by microhardness and conventional mechanical testing. These tests indicate that the deer antler has lower mineral content than bones of the appendicular skeleton. The aim of this study was to examine if significant differences exist in the indentation properties of deer antler when tested under dry and moist conditions by nanoindentation.

Methods. One dry white tail mule deer antler midstem was sectioned and 2 antler blocks (approximately 4 mm thick) were obtained. Each specimen was glued in a custom-made polycarbonate holder. The specimen was polished and briefly sonicated. The specimens were dried in an oven at 45˚C for 120 mins and then set aside for 2 days. The polycarbonate holder was inserted into the receiving table of the nanoindenter (Nano-XP, MTS, Oakridge, TN). The calibration of the indenter and tip was ascertained on fused silica on the day prior to the indentation tests. Indent locations were selected under the microscope of the nanoindenter. In this study, we report two types of indent arrays. The first array, made on the first specimen, consisted of indents that spanned from the periosteal to the endosteal surface, and were spaced at approximately every 40 μm. Intentionally, no adjustment was made for osteonal or interstitial areas, thus resulting in averaging of any differences of indentation properties. However, the antler specimen had a dense arrangement of osteons with little interstitial bone. In the second array, made on the second specimen, localized indents (over an area of approximately 150 X 300 μm) were made at two locations. These localized indents were made primarily on two large osteons. In order to locate indentation sites, marker indents were made to a depth of 4000 nm. For the first array, one marker indent each was placed approximately 150 μm from the periosteal and endosteal surface. This indent created by the Berkovich tip made a sharp cut in the antler and could later be clearly seen under the nanoindenter's microscope. The indents to compare the moist and dry conditions were placed approximately on the line described by these marker points. In the second array (more localized), one marker indent was placed in the two locations of interest and the dry and wet indents were made to start approximately 150 μm away from this indent. The selected location of the indents were examined under the microscope prior to test and indents that fell on a large void or Haversian canal, were deleted from the test array. Indents were made at a constant displacement of 10 nm/s to a target depth of 500 nm first under dry conditions and then under moist conditions. The number of indents on each specimen is listed in Table 1.

	n	Dry	n	Moist
Specimen 1				
modulus (E)	59	16.2 ± 7.05	48	10.81 ± 5.65
hardness (H)		0.19 ± 0.07		0.23 ± 0.14
Specimen 2, Location 1				
modulus (E)	25	18.1 ± 1.8	23	10.1 ± 2.8
hardness (H)		0.5 ± 0.1		0.17 ± 0.07
Specimen 2, Location 2				
modulus (E)	25	20.5 ± 2.2	25	11.22 ± 3.97
hardness (H)		0.55 ± 0.13		0.19 ± 0.04

Table 1

The specimens were hydrated with distilled water over a period of 5 hours. The specimen was not soaking in water but the drip rate was adjusted so the surface of the specimen was barely moist and no large water patches were seen on the surface. Indent locations for moist testing were now selected in close proximity of the marker indents. For the periosteal to endosteal array, a line approximately parallel and at about 50 microns away from the original dry test locations was selected. For the localized array, the indent for moist testing were placed approximately 30 microns away from the dry indents in a 5X5 array. The Oliver-Pharr method was used to calculate the indentation modulus and hardness from the unloading curve at peak displacement. The data were analyzed by ANOVA with pairwise comparisons being made by the Tukey-Kramer method.

Results. The results of the estimated indentation properties (GPa) are summarized in Table 1. There was an approximately 33-45% reduction in the indentation modulus of the dry specimens when tested under moist conditions. In all specimens, there was a significant difference ($p<0.001$) between the indentation modulus and hardness under dry versus moist conditions. The only exception was the lack of difference in hardness for Specimen 1.

Discussion. The deer antler has been used extensively in the past to study the relationship between mineralization and mechanical properties. However, indentation modulus by nanoindentation has not been reported. The indentation modulus values that are presented in this report are only specific to the deer sample used in the current study. The values of moist indentation modulus are slightly higher to those reported by Currey[3] who used conventional mechanical tests. In this study, we noted that the level of the surface of the specimen would be raised by approximately 80,000 nm when a specimen was fully hydrated and equilibrium was reached. We have not observed this dimensional change in our previous frozen specimens and attribute it to drying out and reabsorption of water by the dry specimen. In this study, we choose not to impose a peak load hold period for this specific reason. The issue here is the relative rate of creep compared to the unloading rate imposed by the indenter. If the rate of creep is significantly smaller than the rate of unloading, this creep behavior will have small effects on the modulus. In theory, only 2 points which are in the initial part of the unloading curve are required to generate an indentation modulus value using the Oliver-Pharr method, however typically the first 50% of the unloading curve is used to calculate the indentation modulus. The time-dependent behavior of deer antler needs further investigation. Estimates of indentation properties from nanoindentation on specimens with low level of mineralization should report all testing parameters to allow for interpretation of results.

Acknowledgement

Supported by College of Dentistry start up funds.

References

1. Hengsberger S, Kulik A, Zysset P. Nanoindentation discriminates the elastic properties of individual human bone lamellae under dry and physiological conditions. Bone 2002; 30:178-184.
2. Rho J-Y, Pharr GM. Effects of drying on the mechanical properties of bovine femur measured by nanoindentation. J of Mat Sc, Materials in medicine 1999; 10:485-488.
3. Currey JD. The effect of porosity and mineral content on the Young's modulus of elasticity of compact bone. J Biomech 1988; 21:131-139.

The authors have no conflict of interest.

P-10

Effects of Risedronate and Calcitriol on the Structure and Mechanical Properties of Cancellous Bone in Glucocorticoid-treated Rats

J. Iwamoto[1], A. Seki[2], T. Takeda[1], C-L. Shen[3], J.K. Yeh[4]
[1]Department of Sports Medicine, Keio University School of Medicine, Tokyo, Japan; [2]Hamri Co., Ltd., Tokyo, Japan; [3]Department of Pathology, Texas Tech University Health Science Center, TX, USA; [4]Metabolism Laboratory, Department of Medicine, Winthrop-University Hospital, NY, USA
E-mail: jiwamoto@sonata.plala.or.jp

Glucocorticoids (GCs) clearly induce osteoporotic changes in cancellous bone. The purpose of the present study was to examine the effects of risedronate (Ris) and calcitriol (Cal) on the structure and mechanical properties of cancellous bone in GC-treated rats. Ninety female Sprague Dawley rats, 4 months of age, were randomized by the stratified weight method into nine groups of 10 rats each according to the following treatment schedule: 4-week intact control, and 4-week GC administration with 4-week concomitant administration of vehicle, Ris, Cal, or Ris+Cal as preventive treatment, and 8-week GC administration with 4-week administration of vehicle, Ris, Cal, or Ris+Cal as therapeutic treatment initiated after 4-week administration of GC. The GC (methylprednisolone sodium succinate, 5.0 mg/kg, s.c.), Ris (10 μg/kg, s.c.), and Cal (0.1 μg/kg, p.o.) were administered 3 times a week. At the end of the experiment, two-dimensional (2-D) bone histomorphometric and 3-D micro-computed tomographic analysis of cancellous bone of the proximal tibial and distal femoral metaphyses, respectively, were performed and the mechanical properties of the distal femoral metaphysis were evaluated by compression test. Both 4- and 8-week GC administration resulted in a decrease in 2-D cancellous bone volume (BV/total tissue volume [TV]). However, the decrease in 3-D cancellous BV/TV and maximum load was not observed until 8-week GC administration had elapsed. 2-D and 3-D cancellous BV/TV were increased by preventive and therapeutic Ris treatment. 2-D cancellous BV/TV loss was attenuated and 3-D cancellous BV/TV loss was prevented by preventive Cal treatment, whereas both 2-D and 3-D cancellous BV/TV were increased by therapeutic Cal treatment. Both Ris and Cal treatment had a more pronounced effect on 3-D cancellous BV/TV than on 2-D cancellous BV/TV. Both preventive and therapeutic Ris and Cal treatment increased maximum load to a similar extent, and a significant correlation was found between maximum load and 3-D trabecular number and separation. No apparent additive effects of Ris and Cal were observed on any of the measured parameters. The present study showed that deterioration of 3-D cancellous bone structure and the mechanical properties of the bone occurred after the appearance of 2-D cancellous bone loss in GC-treated rats, and that although Ris had a more pronounced effect on cancellous bone structure than Cal in our dose setting, both preventive and therapeutic Ris and Cal treatment increased the maximum load of the distal femoral metaphysis to a similar extent. Improvement in 3-D cancellous bone structure might significantly contribute to improvement in the mechanical properties of the bone in GC-treated rats.

The authors have no conflict of interest.

P-11

Molecular Genetic Studies of Gene Identification for Osteoporosis: The 2004 Update

*Y-J. Liu[1], H. Shen[1], D-H. Xiong[1], P. Xiao[1], L-H. Li[1], R.R. Recker[1], H-W. Deng[1,2,3]
[1]Osteoporosis Research Center, Creighton University Medical Center, Omaha, NE, USA; [2]The Key Laboratory of Biomedical Information Engineering of Ministry of Education and Institute of Molecular Genetics, School of Life Science and Technology, Xi'an Jiaotong University, Xi'an, P. R. China; [3]Laboratory of Molecular and Statistical Genetics, College of Life Sciences, Hunan Normal University, Changsha, Hunan 410081, P. R. China
E-mail: jun@creighton.edu

This review article summarizes comprehensively the most important and representative molecular genetics studies of gene identification for osteoporosis published within the past two years (2003-2004). It constitutes an update of our previous review article published in *Journal of Endocrinology*, which summarized available data up to the end of 2002 (Liu et al., *J Endocrinol* 2003; 177:147-196). As in our first review, evidence from candidate gene association studies and genome-wide linkage studies in humans, as well as QTL (quantitative trait locus) mapping animal models are reviewed separately.

Transgenic and knockout murine models relevant to osteoporosis are also summarized. A notable extension in this update is the inclusion of functional genomic studies (including DNA microarray and proteomics studies), owing to the rapid progress in this area and its promising prospects in understanding of the biochemistry of proteins, processes and pathways relevant to osteogenesis and osteoporosis. The results of important studies are entered in tables for the purpose of comparison and ease of reference. Comments are made on the most notable findings and representative studies for their potential influence and implications on our present understanding of genetics of osteoporosis. The format adopted by this review should be ideal for accommodating future new advances and studies in a fairly young field that is still rapidly developing.

The authors have no conflict of interest.

P-12

Mandibular Bone Mass and Geometry of C57BL/6J (B6) and B6.C3H-4T (4T) Mice

I.F. Meta[1], S.S. Huja[1,2], S.J. Warden[3], C.H. Turner[4]
[1]Section of Oral Biology and [2]Orthodontics, College of Dentistry, Ohio State University, Columbus, OH, USA; [3]Department of Physical Therapy and [4]Department of Orthopaedic Surgery, Indiana University School of Medicine, Indianapolis, IN, USA
E-mail: meta.2@osu.edu

Introduction. Skeletal mass and density are regulated by genetic factors. Bones which express a phenotype of higher mass could be more mechanosensitive than those with lower bone mass. Quantitative trait loci (QTL) has mapped chromosome 4 and related it to femoral width. These findings lead to the development of B6.C3H-4T (4T) mice[1]. These mice carry the genetic information of the C57BL/BJ (B6) strain, but have chromosome 4 of the C3H/HeJ (C3H) strain. Ulnae of this 4T strain were reported to have greater cortical area than B6 mice. The mandible has been divided into several functional regions. One important division is the ramus and the body of the mandible[2]. Although the influence of chromosome 4 in the mechanosensitivity of long bones was reported[1], its effects on the mandible are unknown. The purpose of this study was to measure the mandibular bone mass and geometry of 4T mice and compared them with those of B6 mice.

Materials and methods. Eight-week-old female (f) and male (m) B6 (n_f=*5;* n_m=*8*), and 4T (n_f=*13;* n_m=*13*) mice were examined. Hemimandibles were dissected and cleared of soft tissue. These specimens were embedded in methyl methacrylate for sectioning with a diamond wire saw (Delaware Diamond Knives, Wilmington, DE, USA). Before sectioning the specimens, Faxitron lateral view images of all the hemimandibles were obtained. These images were digitalized with a high resolution scanner and loaded in a computer imaging program (Analysis Image Processing, Olympus, Melville, NY, USA). The lateral view of the hemimandible was divided into an anterior and a posterior region (Figure 1). The same specimens (*n*=*57*) were quantified after two weeks to determine the measurement error (~3%). The total area was calculated as the sum of the anterior and posterior areas. Next, four consecutive sections (80 μm) of each hemimandible starting at the distal side of the third molar and progressing anteriorly, were selected by their morphology (Figure 2). Their bone area was assessed with Merz grid at 200x magnification with a microscope

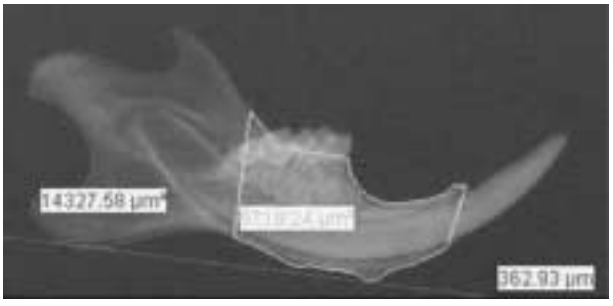

Figure 1. Lateral view of the hemimandible. Anterior and posterior regions divided by a line distal to the third molar and perpendicular to the base of the mandible.

Figure 2. Microscope images of the four consecutive mandibular cross-sections at 40x magnification.

(BX51 Olympus, Melville, NY, USA). The data collected from the four cross-sections of each hemimandible were averaged to estimate the cross-sectional area (CSA) of each specimen. Hemimandibles were the coronoid process was not intact were excluded from analyses. Mann-Whitney test was used to compare area parameters of the 4T and B6 hemimandibles from the same side.

Results.

	MALE (Means ± SE, mm^2)				**FEMALE** (Means ± SE, mm^2)			
	Right		**Left**		**Right**		**Left**	
	4T	B6	4T	B6	4T	B6	4T	B6
CSA	1.53 (.025)^a n=10	1.48 (.026)^a n=7	1.54 (.035)^a n=8	1.51 (.034)^a n=6	1.67 (.017)^c n=8	1.43 (.038)^c n=5	1.69 (.036)^a n=10	1.54 (.101)^a n=3
Ant. Area	14.84 (.120)^a n=8	14.86 (.192)^a n=7	15.01 (.247)^a n=7	15.28 (.300)^a n=7	14.61 (.282)^a n=9	14.77 (.307)^a n=5	15.21 (.194)^a n=11	14.31 (.539)^a n=3
Post. Area	22.90 (.462)^a n=8	21.86 (.344)^a n=7	23.21 (.316)^b n=7	21.75 (.244)^b n=7	21.17 (.343)^c n=9	18.12 (.459)^c n=5	20.70 (.313)^b n=11	18.55 (.151)^b n=3
Total Area	37.74 (.498)^a n=8	36.73 (.518)^a n=7	38.21 (.489)^a n=7	37.03 (.476)^a n=7	35.78 (.276)^c n=9	32.90 (.582)^c n=5	35.91 (.334)^b n=11	32.86 (.402)^b n=3

^{a}p>.05; ^{b}p<.05; ^{c}p<.01

Discussion. The 4T female hemimandibles had a 10-17% greater CSA than the B6. In lateral view, the 4T had 11-17% greater posterior area than the B6, with smaller (1-6%) differences in the anterior area. These data suggest that 4T mice may be more mechanosensitive to physiological loads than B6 mice. The three-dimensional bone mass distribution evidenced in the anterior portion could be because of the strain direction during chewing. The greater differences in the right side parameters compared with those in the left side, may be attributed to the limited sample size of the B6 group. The parameters studied in the male specimens did not show the differences reported for the female hemimandibles between groups. Therefore, it could be possible that the effects of chromosome 4 on the bone mass and geometry observed in female mice were sex-specific. Robling et al.[1] reported a ~10% difference in the ulnar midshaft cortical area between 4T and B6 female mice.

Conclusions. The data obtained suggest that 4T mice have a greater bone mass than B6 mice. This difference was larger in the female than in the male. Therefore, we conclude that the mechanosensitivity of 4T mice extends to the osseous tissues in the craniofacial region.

References

1. Robling AG, Li J, Shultz KL, Beamer WG, Turner CH. Evidence for a skeletal mechanosensitivity gene on mouse chromosome 4. Faseb J 2003; 17:324-326.
2. Klingenberg CP, Leamy LJ, Routman EJ, Cheverud JM. Genetic architecture of mandible shape in mice: effects of quantitative trait loci analyzed by geometric morphometrics. Genetics 2001; 157:785-802.

The authors have no conflict of interest.

P-13

Association of Ehlers Danlos Syndrome (EDS) With Temporary Brittle Bone Disease (TBBD) From Fetal Immobilization

M. Miller
Department of Pediatrics, Ob/Gyn, and Biomedical Engineering, Wright State University, Dayton, OH, USA
E-mail: srmmem@aol.com

TBBD was described by Paterson in 1993 as an intrinsic bone disorder with unexplained fractures in the first year of life. Paterson noted an association of TBBD with joint hypermobility in 66% of parents of infants with TBBD. In 1999 it was hypothesized that the primary cause of TBBD was fetal immobilization. This hypothesis is in accord with the Utah paradigm as posited by Frost (Anat Rec 262:398-419) and is an extension of the Utah paradigm to the fetal period of bone formation. Most child abuse protectionists believe that TBBD does not exist and is a ruse for child abuse. A review of 60 cases of infants with TBBD from fetal immobilization showed that 6 cases also had EDS of the subtype associated with joint hypermobility and easy bruising (10%). This is significantly higher than the general population frequency of EDS of about 1 in 5,000 (Canadian EDS Association). This striking association of EDS with TBBD and Paterson's observation of a striking association of joint hypermobility in parents of infants with TBBD suggest that joint hypermobility may be a predisposing factor to TBBD from fetal immobilization.

This association may be explained by the observation that compared to fetus with normal joint mobility, a fetus with EDS experiences diminished skeletal bone loading when they push off the maternal uterine wall with their arms and legs, as these extremities would be more prone to collapse in flexion and not transmit the load. The association of EDS with TBBD supports the concept that fetal bone loading is an important determinant of fetal bone strength.

The author has no conflict of interest.

P-14

Three-Years Bisphosphonate Treatment Increased Bone Strength by Increasing Osteonal Degree of Mineralization in Spite of Increased Microdamage Accumulation in Dog's Rib

S. Mori, S. Komatsubara, T. Mashiba, T. Manab
Department of Orthopedic Surgery, Faculty of Medicine, Kagawa University, Japan
E-mail: stmori@kms.ac.jp

It is well recognized that suppression of bone resorption affects mechanical properties of bone by changing bone quality as well as bone volume and architecture. Bone quality consists of microdamage accumulation, degree of mineralization of bone and cross-links of collagen. However, the relationships

of these quality factors on bone strength are still unknown. We have measured microdamage and degree of mineralization in dog's rib following 3-years bisphosphonate treatment in order to evaluate their relative effects on bone mechanical properties.

Materials and methods. Twenty-nine beagels of 1 year old were treated by either control vehicle(CONT), incadronate disoudium (3rd generation bisphosphonate, Ymanouchi Japan) 0.3 mg/kg/day, p.o.(LOW: x 2.5 clinical dose) or 0.6 mg/kg/day(High: x 5 clinical dose) for three years and sacrificed after double labeling. Bone mineral density of the 9th rib was measured using pQCT, 3-point bending test was applied and mechanical properties such as ultimate force, stiffness and work to failure were derived; then ultimate stress, elastic modulus, toughness were further calculated by standardization using CSMI. The specimens were processed for histomorphometrical evaluation and cortical area, activation frequency, microdamage density and osteonal degree of mineralization were derived.

Results. Ultimate force, stiffness and work to failure were significantly increased in LOW and HIGH compared to CONT, while no statistical significance was found in ultimate stress, elastic modulus or toughness among the groups. Mean osteonal degree of mineralization and microdamage density were significantly higher in Bs. treatment groups compared to CONT. Cortical area did not differ among the groups, while cortical BMC significantly increased in Bs. treatment groups. Activation frequency was significantly lower in Bs. treatment groups compared to CONT.

Discussion. Three year suppression of bone turnover by Bs. treatment increased both microdamage accumulation and degree of mineralization, and increased mechanical strength of the bone. Microdamage accumulation increases depending on the extent of suppression of bone remodeling and cause reduced intrinsic material properties. Suppression of bone remodeling also increases bone strength by increasing the degree of mineralization. Increased accumulation of microdamage and degree of mineralization following Bs. treatment works oppositely on bone strength. In this study, negative effect of increased microdamage density on intrinsic material properties were compensated by the increased osteonal degree of mineralization. It is also reported that 1 year of alendronate treatment decreased toughness, suggesting that the effect of Bs. treatment on bone strength may differ depending on the treatment period, dose, age, or bone turnover.

The authors have no conflict of interest.

P-15

Role of Structural Size Scales in the Aging-Related Deterioration of the Toughness of Cortical Bone and Dentin

R.K. Nalla[1], R.O. Ritchie[1], J.W. Ager III[1], J.H. Kinney[2]
[1]Lawrence Berkeley National Laboratory, Berkeley, CA, USA, [2]University of California, San Francisco, CA, USA
E-mail: rknalla@lbl.gov

Aging-related deterioration of the fracture properties of mineralized tissues, coupled with higher life expectancy, is partly responsible for the increased incidence of fractures in the elderly; consequently, an understanding of why these fracture properties degrade with age is essential. Here, we evaluate such changes in two tissues – cortical bone and dentin, the most abundant tissue in the tooth. At the smallest structural length scales (less than 1 μm), the composition and structure of dentin is similar to that of bone, i.e., a composite of nanocrystalline apatite mineral and type-I collagen. At larger length scales, the similarities between dentin and bone are less obvious, as the specialized functions of these tissues require remarkably different microstructures.

Ex vivo fracture experiments were performed to quantitatively assess the effect of age on cortical bone. Because cortical bone exhibits rising crack-growth resistance with crack extension in the proximal-distal orientation, the toughness was evaluated in terms of resistance-curve (R-curve) behavior for bone taken from a wide range of age groups (34-99 years). Using this approach, both the crack-initiation and crack-growth toughness were found to deteriorate with age; the initiation toughness decreased some 40% from 40 to 100 years, while the growth toughness was effectively eliminated over the same age range. Changes in the cross-linking chemistry (at the nanostructural size scale) evaluated using UV-Raman spectroscopy correlated better with changes in the initiation toughness ($p=0.04$), but not the growth toughness ($p=0.23$). Examination of cracks with X-ray tomography revealed that degradation of crack bridging, a potent extrinsic toughening mechanism involving uncracked material (several hundred μm in dimension, i.e., at the microstructural size scale) in the crack wake that reduces the stresses experienced at the crack tip, was responsible for the reduction in crack-growth toughness.

In dentin, where remodeling is absent, one of the age-related changes occurring is the gradual occlusion of the 1-2 μm tubules, which are the main microstructural feature of the tissue. Such occlusion ultimately leads to an optical transparency, forming so-called transparent dentin. In this study, *ex vivo* fracture experiments were performed on normal, or young (donor age: 23.9 ± 7 years) and transparent dentin (donor age: 80.4 ± 10.4 years). Fracture toughness (single-value toughness obtained due to sample size restrictions) was again significantly altered ($p=0.03$) with age, with transparent dentin having about 20% lower toughness; this could be associated with a reduction in crack bridging. We believe that the occlusion of the tubules with mineral acts to lower the tendency for microcrack nucleation there. In the absence of microcrack nucleation well ahead of the main crack tip, crack bridges are less likely to form, which in turn lowers the fracture toughness of the dentin.

Thus, two tissues with similar structure at the molecular level, but remarkably different microstructures (initially different, and further changes with age), both show age-induced deterioration in the fracture properties that can be related to changes at the microstructural size scales.

The authors have no conflict of interest.

P-16

Inhibin is a Novel Endocrine Stimulator of Bone Mass, Architecture, and Strength, Through Effects on Bone Formation

*D.S. Perrien[1], N.S. Akel[1], P.K. Edwards[1], A.A. Carver[2], R.A. Skinner[2], F.L. Swain[2], L.J. Suva[2], D. Gaddy[1]
[1]Physiology and Biophysics and [2]Center for Orthopaedic Research, Orthopaedic Surgery, University of Arkansas for Medical Sciences, Little Rock, AR, USA
E-mail: perriendaniels@uams.edu

Hypogonadism causes a rapid decline in bone mass leading to osteoporosis. We have previously demonstrated that Inhibin A (InhA) suppresses osteoblast and osteoclast differentiation *in vitro*. This led to the hypothesis that Inhibins maintain bone mass *in vivo* by suppressing bone turnover. To test this hypothesis, the GeneSwitch system of mifepristone (MFP) inducible human InhA overexpression was utilized. Six-month-old male mice at peak bone mass underwent either sham (Sham) or orchidectomy (Orch) and subcutaneous placement of a time-release pellet containing MFP or vehicle (Veh). All mice were sacrificed on day 28. Using *ex vivo* microCT and finite element modeling, as well as direct compressive strength testing, MFP-induced overexpression of InhA prevented Orch-induced loss of trabecular bone volume, microarchitecture and strength ($p<0.05$) in the proximal tibia and the L5 vertebrae. In addition, InhA improved these measures in intact Sham operated mice (all $p<0.05$). Systemic bone resorption, measured by serum collagen C-telopeptide cross-links, was significantly increased by Orch ($p<0.05$ vs. Sham) but unaffected by InhA, regardless of gonadal status. Histomorphometric analysis of tibial trabecular bone revealed that InhA did not affect any static osteoclast or osteoblast parameters, but increased mineral apposition and bone formation rates in both Sham and Orch mice (all $p<0.05$). Collectively, these data are the first to demonstrate that InhA, a peptide hormone normally produced by the gonad, is a novel endocrine stimulator of bone formation via selective effects on osteoblast function, and suggest its signaling pathway warrants further study as a potential therapy for osteoporosis.

The authors have no conflict of interest.

P-17

RUNX2 Transcription Factor Regulates MMP9 in Bone Metastatic Cancer Cells and Controls Cell Invasion

*J. Pratap[1], A. Javed[1], L.R. Languino[2,3], A.J. van Wijnen[1], J.L. Stein[1,3], G.S. Stein[1,3], J.B. Lian[1,3]
Departments of Cell Biology[1], Cancer Biology[2], and Cancer Center[3], University of Massachusetts Medical School, Worcester, MA, USA
E-mail: jitesh.pratap@umassmed.edu

Runx2 (Cbfa1/AML3) is a master gene transcription factor, regulating numerous target genes essential for processes required for bone development;

for example, cell growth (p21), vascular invasion (VEGF), bone matrix formation (BSP, OC, OP) and turnover of bone tissue (MMP13). Runx2 integrates signals transduced from growth factors (e.g., IGF-1, TGFβ/BMP) and the extracellular matrix (e.g., integrin and c-src signaling) by forming Runx2 co-regulatory protein complexes in subnuclear domains mediated by a Runx2 targeting signal (NMTS). Notably, these signaling pathways are upregulated in metastatic prostate and breast cancer cells. Our studies show that Runx2 expression is induced in these cell lines compared to cells derived from primary tumors. However, the function of Runx2 in tumor progression and in the metastatic lesions is still not understood. By cDNA expression array analysis, we identified MMP9 as a novel downstream target of Runx2. Upregulation of MMP9 expression has been implicated in invasion and metastasis of breast and prostate tumors. Like MMP13, MMP9 expression is nearly depleted in Runx2 mutant mice. *In vivo* analysis by chromatin immunoprecipitation assay and *in vitro* by EMSA revealed recruitment of Runx2 to the MMP9 promoter. We show by mutational analysis that the Runx2 site mediates transactivation of the MMP9 promoter in osteoblasts (MC3T3- E1) and non-osseous (HeLa) cells. Overexpression of Runx2 by adenovirus delivery in poorly metastatic (MCF-7) and in metastatic breast (MDA-MB-231) and prostate (PC3) cancer cell lines significantly increases endogenous levels of MMP9. Knockdown of Runx2 by RNA interference decreases MMP9 expression, as well as other Runx2 target genes, including MMP13 and VEGF. Importantly, we have demonstrated using a cell invasion assay that Runx2 regulated MMP9 levels are functionally related to the invasion properties of cancer cells. These results are consistent with Runx2 control of multiple genes that contribute to the metastatic properties of cancer cells and their activity in the bone microenvironment. We propose that the relationship between expression of metastatic markers and the invasive behavior of cancer cells may be linked to the integration of regulatory signals that are mediated by Runx2.

The authors have no conflict of interest.

P-18

Re-expression of DMP1 in the Osteoblast Lineage Rescues the Mineralization Defect in the Osteocyte Lacuno-canalicular System

*H.F. Rios[1], Y. Lu[1], V. Dusevich[1], D. Nicolella[2], S. Kotha[1], S. Zhang[1], Y. Xie[1], L. Ye[1], M.D. McKee[3], J.D. Eick[1], L.F. Bonewald[1], J.Q. Feng[1]
[1]Oral Biology, School of Dentistry, UMKC, Kansas City, MO, USA; [2]Mech and Matls Engr, SW Research Institute, San Antonio, TX, USA; [3]McGill University, Montreal, Quebec, Canada
E-mail: hfr4e6@umkc.edu

Deletion of *Dentin Matrix Protein 1 (DMP1)* results in a severe osteomalacia-like phenotype. Previously, it has been suggested that osteocytes may be involved in the maturation and mineralization of the osteoid matrix by secreting specific matrix molecules. *DMP1* immunolocalization has been observed along the canalicular walls using TEM and light microscopy. To gain further insight into the mineralization abnormalities, the osteocyte lacuno-canalicular system of WT and *Dmp1* KO mice was analyzed using procion red injection, AFM, TEM, backscatter SEM, and resin casted SEM techniques. These experiments showed that the osteocyte lacuno-canalicular system in the Dmp1 KO mice is irregular and disorganized. In addition, the dendrite membrane surfaces appeared buckled and ridged, while the osteocyte body is enlarged. To determine if re-expression of *DMP1* in the osteoblast lineage would rescue the KO phenotype, 5 independent transgenic lines overexpressing *DMP1*, driven by a 3.6 kb rat type 1α1 collagen promoter, were generated for crossing with *Dmp1* KO mice. Re-expression of *DMP1* using this promoter rescued the phenotype by 1 month of age. High *DMP1* protein expression was confirmed in both osteoblasts and in osteocyte canaliculi in the rescued mice. Interestingly, no phenotype was observed when *DMP1* was overexpressed on a normal background. Together these data show that *DMP1* is an essential extracellular matrix protein for the establishment of normal osteocyte and lacuno-canalicular morphology. These findings identify *DMP1* as a critical local regulator of mineral incorporation into osteoid and highlight its unique role in the molecular pathway for mineralization in bone. Work supported by NIH/NIDCR T32DE07294 and DE13480.

Dr. Bonewald receives royalties from licensing of MLO cells.
All other authors have no conflict of interest.

P-19

The Effect of Oxygen Tension on the Colony Formation and Proliferation of Human Connective Tissue Progenitor Cells in Primary Tissue Culture

*S. Villarruel[1,2], C. Boehm[1], M. Pennington[1], K. Powell[1], G. Muschler[1]
[1]Department of Biomedical Research and The Orthopaedic Research Center Cleveland Clinic Foundation; [2]Biomedical Engineering Department, Case Western Reserve University Cleveland, OH, USA
E-mail: muschlg@ccf.org

Bone marrow contains connective tissue progenitor cells (CTPs) that can be activated to form new connective tissues including; bone, cartilage, tendon, muscle, marrow stroma, and fat. The heterogeneous CTP population can be characterized by analysis of the progenitor cells capacity to both form and expand colonies using a colony-forming unit (CFU) assay. The number of CFUs found in a population reflects both the number of CTPs in the population and the activation efficiency of these cells under the culture conditions. Proliferation can be assayed in each colony, based on the number of cells in each colony at a fixed time following activation. Optimization of the use of CTPs in therapeutic cellular grafts requires an improved understanding of the bone healing environment and the response of CTPs to those conditions. One of the most characteristic features of the fracture site or site of cell transplantation is hypoxia, due to an imbalance between the metabolic demand of local cells and the initial lack of vascularization within the fracture/graft site. The response of CTPs to a low oxygen tension environment is therefore critical to the biological performance of these cells following transplantation. This study assessed the effect of oxygen tension on CTPs using quantitative analysis of CFUs under four oxygen conditions. Using an approved IRB consent protocol (#1309) bone marrow was harvested from the iliac crest of fifteen patient donors. Bone marrow derived cells were cultured under conditions that promote an osteoblastic phenotype for six days at four different oxygen tension levels: 20%, 10% 5%, and 1% (corresponding to PO2=152 mmHg, PO2=76 mmHg, PO2=38 mmHg, and PO2=7.6 mmHg, respectively). The cultures were then fixed using 1:1 acetone/methanol and stained with DAPI, to fluorescently label nuclei. CTP cultures were imaged using a 2048x3072 Quantix K6303E 12 bit digital camera (Roper Scientific) attached to a Leica DMXRA motorized microscope and controlled by imaging software Metamorph (v4.6). Individual images were collected at 512 x 768, 8-bit gray level, using a 10x objective and then montaged together (20 columns x 24 rows) to create one image of the entire cell culture well (2cm x 2cm square). The image analysis software used for quantitative characterization of CTPs was developed using algorithms written in the C/C++ programming language and Motif X-Windows TM environment. In fifteen patient donors, a total of 9,168 colonies containing a total of 224,631 cells were assayed. The colony forming efficiency (CFE), based on the mean number of colonies at each oxygen tension was increased at lower oxygen tensions (1%, 5%, 10%) when compared to CTPs cultured at 20%. Oxygen tension 5% is fifty seven percent more efficient than the baseline value of 20% oxygen with a p-value<0.0003. In addition both 1% oxygen and 10% oxygen are also higher than the baseline reflecting an increased activation rate, even at 1% oxygen. All oxygen tensions possess a similar cells per colony distribution trend, but both 5% and 10% oxygen are markedly greater than oxygen tensions 1% and 20%, which themselves are comparable. In this setting colonies containing 8, 16, 32 . . . cells can be viewed as having undergone 3, 4, 5 . . . cycles of proliferation. The effective proliferation rate was significantly greater at lower oxygen tension (1, 5, 10%) than at 20% O2 (p-value< 0.0002) despite large variation between individual CFUs at all oxygen tensions. The wound healing environment, in particular oxygen tension, has a great impact on composite cellular grafts used in the clinical setting. Using the CFU assay we have demonstrated that low oxygen tension conditions, even down to 1% oxygen may actually increase CTP activation and also increase the proliferation of progenitor cells in colonies. These findings have important implications in the biological response and survival of CTPs following local trauma or transplantation and also influence the design and development of delivery systems for CTPs in tissue engineering applications. These data suggest that CTPs have the biological trait of both tolerance for very low oxygen tension conditions and even the tendency to be induced to greater rates of activation and greater rates of proliferation under low oxygen tension conditions. These features may enhance their capacity to survive and compete with other local cells in the wound healing environment or other transplantations.

The authors have no conflict of interest.